Ionic mechanisms underlying tonic and burst firing behaviour in subfornical organ neurons: a combined experimental and modeling study

Abbreviated title: Model of SFO Neurons

Laura Medlock[1], Lauren Shute[2], Mark Fry[2], Dominic Standage[1*], and Alastair V. Ferguson[1*]

[1]Center for Neuroscience Studies, Queen's University, Kingston, ON, Canada K7L 3N6
[2]Department of Biological Sciences, University of Manitoba, Winnipeg, MB, Canada R3T 2N2
*DS and AVF contributed equally to this work as co-senior authors

Correspondence to: Dr. Alastair V. Ferguson
Center for Neuroscience Studies
Department of Biomedical and Molecular Sciences, Queen's University
Botterell Hall, 18 Stuart Street, Kingston, ON K7L 3N6
Tel: (613) 533-2803; Fax: (613) 533-6840; Email: avf@queensu.ca

Conflict of Interest: No conflicts to report.

Acknowledgements: This work was supported by the Canadian Institutes for Health Research (CIHR) grant MOP12192 to AVF.

ABSTRACT

Subfornical organ (SFO) neurons exhibit heterogeneity in current expression and spiking behaviour, where the two major spiking phenotypes appear as tonic and burst firing. Insight into the mechanisms behind this heterogeneity is critical for understanding how the SFO, a sensory circumventricular organ, integrates and selectively influences physiological function. To integrate efficient methods for studying this heterogeneity, we built a single-compartment, Hodgkin-Huxley type model of an SFO neuron that is parameterized by SFO-specific *in vitro* patch clamp data. The model accounts for the membrane potential distribution and spike train variability of both tonic and burst firing SFO neurons. Analysis of model dynamics confirms that a persistent Na^+ and Ca^{2+} current are required for burst initiation and maintenance, and suggests that a slow-activating K^+ current may be responsible for burst termination in SFO neurons. Additionally, the model suggests that heterogeneity in current expression and subsequent influence on spike afterpotential underlies the behavioural differences between tonic and burst firing SFO neurons. Future use of this model in coordination with single neuron patch clamp electrophysiology, provides a platform for explaining and predicting the response of SFO neurons to various combinations of circulating signals, and thus elucidating the mechanisms underlying physiological signal integration within the SFO.

NEW & NOTEWORTHY

Our understanding of how the SFO selectively influences ANS function remains incomplete, but theoretically results from the electrical responses of SFO neurons to physiologically important signals. We have built a computational model of SFO neurons, derived from and supported by experimental data, which explains how SFO neurons produce different electrical patterns. The model provides an efficient system to theoretically and experimentally explore how changes in the essential features of SFO neurons affect their electrical activity.

KEY WORDS: subfornical organ, model, Hodgkin-Huxley, bursting, ionic mechanisms

INTRODUCTION

The subfornical organ (SFO) has been shown to be an important site where integration of information from multiple circulating signals takes place and contributes to physiological regulation of the autonomic nervous system (ANS) (Smith and Ferguson 2010). It is well established that SFO neurons are sensitive to a wide range of circulating peptides across traditionally different physiological systems and, consequently, the SFO is able to influence a diverse range of ANS function including water balance, salt-appetite, cardiovascular, immune function, and reproduction (Ferguson and Bains 1996; McKinley et al. 1998; Smith and Ferguson 2010; Zimmerman et al. 2017). Previous studies show that signal integration in the SFO occurs at the single neuron level (Cancelliere and Ferguson 2017; Hattori et al. 1988; Pulman et al. 2006; Tanaka et al. 2001), but comprehensive investigation of this integration, especially across different physiological systems, remains a challenge for patch clamp electrophysiology in view of the extended recording times necessary to evaluate such interactions.

The ability of SFO neurons to integrate and modify physiological function is the result of complex ion channel expression/modulation and its influence on membrane potential. Previous studies indicate that the SFO exhibits heterogeneity in K^+ current expression between different neuronal subpopulations (Anderson et al. 2001; Ono et al. 2005). Several additional currents have also been identified in SFO neurons through *in vitro* whole cell techniques, including multiple Na^+ and Ca^{2+} currents, in addition to conductances such as the Ca^{2+}-activated non-selective cationic current (Ferguson and Bains 1996; Ferguson and Li 1996; Fry and Ferguson 2007; Hiyama and Noda 2016; Kuksis and Ferguson 2015; Washburn et al. 2000a; Washburn and Ferguson 2001b; Washburn et al. 1999b; Yang et al. 2016). Heterogeneity in membrane

properties and current expression likely plays a major role in influencing the two prominent spiking behaviours exhibited by SFO neurons, tonic and burst firing, but little is currently known about differences in ion channel expression between individual SFO neuron subpopulations. Previous studies show that burst firing is found in approximately half of dissociated SFO neurons, appears as a plateau depolarization superimposed with action potentials, and that bursting behaviour is preserved *in vivo* (Washburn et al. 2000b). Although various *in vitro* whole-cell patch clamp studies have investigated the mechanisms of burst initiation and maintenance in SFO neurons (Washburn et al. 2000b; Washburn et al. 1999b), the mechanism underlying burst termination remains unknown. Furthermore, the roles of both tonic and burst firing behaviour in SFO neurons remains unclear, although, in other neuron populations burst firing has been hypothesized to allow for preferential release of neuropeptides (Andrew and Dudek 1983; van den Pol 2012; Washburn et al. 2000b). SFO neurons have been shown to communicate with projection sites in the hypothalamus using the peptide angiotensin II (Ang II) as a neurotransmitter (Li and Ferguson 1993; Smith and Ferguson 2010). Together these findings suggest that deciphering the mechanistic differences between tonic and burst firing may be crucial to our understanding of how SFO neurons release both classical and peptidergic neurotransmitters, the latter of which in particular may play critical roles in the long-term regulation of autonomic outputs.

In this study, we have built a single-compartment, Hodgkin-Huxley type model of an SFO neuron (Hodgkin and Huxley 1952), in order to establish computational methods to integrate with patch clamp electrophysiology. This work not only provides a model to elucidate mechanisms underlying the heterogeneous spiking behaviour of SFO neurons, but also lays the groundwork for future studies to understand the ability of these neurons to integrate multiple

physiological signals. Through analysis of patch clamp data from SFO neurons and quantification of SFO spiking behaviour, we created a model that not only accounts for the membrane potential distribution and spike train variability of both tonic and burst firing SFO neurons, but also offers a physiological explanation for this spiking behaviour and makes testable predictions for future experiments.

MATERIALS & METHODS

Electrophysiology

All animal procedures were approved and in compliance with the Queen's University Animal Care Committee and the University of Manitoba Animal Care Committee, as well as the Canadian Council on Animal Care guidelines. All electrophysiology shown and analyzed in this study was collected in previous studies in cultured, dissociated SFO neurons (Cancelliere and Ferguson 2017; Shute et al. 2016). Solutions and methods for current-clamp electrophysiology were as described by Cancelliere and Ferguson (2017). Activation and inactivation parameters for the currents in our model (see Table 1) were either established from previously published findings (as described in *SFO Neuron Model)* or measured and analyzed from voltage-clamp experiments in SFO neurons (Shute et al. 2016). Briefly, methods for the isolation, measure, and analysis of I_K and I_A were as described by Anderson et al. (2001), but in the presence of 1.0 μM tetrodoxin (TTX), and methods for I_{Na} were as described by Fry and Ferguson (2007).

Membrane Potential & Spiking Behaviour Analysis

We used two standard measures of neuronal activity to quantify differences between tonic (Figure 1A) and burst (Figure 1B) firing in SFO neurons. The first measure was membrane potential distribution modality, which allowed us to account for the bistable membrane potential changes exhibited by burst firing SFO neurons (Washburn et al. 2000b). Modality was assessed for each current-clamp recording by plotting the membrane potential at each time point in a frequency histogram and assessing the resulting distribution shape (Kinard et al. 1999; Sheroziya et al. 2009). The second measure of neuronal activity was the coefficient of variation (CV) of interspike intervals (ISIs), which allowed us to quantify spike train variability (Holt et al. 1996). To accomplish this, ISI times were extracted and CV was calculated for the current-clamp recording of each SFO neuron using the formula $CV = \sigma_{ISI}/\mu_{ISI}$, where σ_{ISI} and μ_{ISI} are the standard deviation and mean of the ISI distribution, respectively. A frequency histogram of all CV values was plotted using a bin size of 0.3 (dimensionless units). The same methods for measuring membrane potential distribution modality and CV were applied to model SFO neurons.

SFO Neuron Model

We developed a minimal, Hodgkin-Huxley type (Hodgkin and Huxley 1952) model of a dissociated SFO neuron (Figure 2A). SFO neurons receive most of their input from the circulation and are known to have small dendritic trees (Dellmann and Simpson 1979; Smith and Ferguson 2010), which are removed during the dissociation technique (Ferguson et al. 1997). Therefore, the model is a single-compartment, spherical soma measuring 10 μm in diameter. The model contains multiple currents reported to be expressed in SFO neurons: a transient (I_{Na}) and persistent (I_{NaP}) Na^+ current (Ferguson and Bains 1996; Fry and Ferguson 2007; Washburn et al. 2000b); a delayed-rectifier (I_K) and transient (I_A) K^+ current (Anderson et al. 2001; Ono et al.

2005; Washburn and Ferguson 2001a); an N-type calcium current (I_{Ca}) (Washburn and Ferguson 2001b); and a non-selective cationic current (I_{NSCC}) (Washburn et al. 2000b; Washburn et al. 1999b). Additional currents that contribute to the model's firing pattern include a slow-activating K^+-current (I_{KS}), leak current (I_L), applied current (I_{app}) and an injected noise current (I_{noise}).

Model Equations

The membrane potential of the model is described by,

$$C_m \frac{dV}{dt} = -(I_{Na} + I_{NaP} + I_K + I_A + I_{Ca} + I_{KS} + I_{NSCC} + I_L) + I_{noise} + I_{app} \ , \quad (1)$$

where C_m = 1.59 μF/cm^2 is the specific membrane capacitance, V is the membrane potential in mV, t is time in ms, I_{app} is injected current in μA/cm^2. To study the effects of noise on these neurons we injected current noise, I_{noise}, in the form of Gaussian white noise with standard deviation, $\sigma_{noise,}$ in μA/cm^2. Individual currents I_γ ($\gamma \in$ {Na, NaP, K, A, Ca, KS, NSCC, L}) are described by,

$$I_\gamma = g_\gamma m^p h^q (V - E_{ion}) \ , \quad (2)$$

where gating variables, *m* and *h*, describe the activation and inactivation of each channel, determining the probability of the channel being open at a given membrane potential. These gating variables are governed by exponents *p* and *q*, which describe the number of activation and inactivation gates for each channel. E_{ion} is the reversal potential of each associated ion and g_γ is maximal conductance associated with current I_γ in mS/cm^2. The E_{Na} and E_K were calculated based on Cancelliere and Ferguson (2017), and E_{Ca} and E_{NSCC} were based on previously reported values (Ono et al. 2001; Roper et al. 2004). SFO neurons typically exhibit a high input resistance of around 1 GΩ and a resting membrane potential between -57mV and -65mV (Ferguson and Bains 1996). In our model, these electrophysiological properties are accounted for by the leak current, I_L, such that E_L = -65 mV and $g_L = 1/R_m$ = 0.318 mS/cm^2, where R_m = 3142 Ω×cm^2 is the

specific membrane resistance for the given patch of cell membrane calculated from an input resistance of 1 GΩ and cell area of 3.142×10^{-6} cm^2 (using a diameter of 10 μm as previously stated). The gating variables (*m* and *h*) associated with each current follow

$$\frac{dx}{dt} = \frac{x_\infty - x}{\tau_x}, \quad (3)$$

where *x* refers to the gating variable (*m* or *h*) and τ_x is the corresponding time constant in milliseconds (ms). The steady-state activation and inactivation function x_∞ is given by

$$x_\infty = \frac{1}{1 + exp^{\frac{(V - \emptyset_x)}{-k_x}}}, \quad (4)$$

where $\emptyset_x$ and k_x are the half activation/inactivation voltage and slope of gating variable *x*, respectively. Activation and inactivation parameters $\emptyset_x$ and k_x for each current are based on previously published findings in SFO neurons for I_{NaP}, I_{Ca}, and I_{NSCC} (Anderson et al. 2000; Fry and Ferguson 2007; Kuksis and Ferguson 2015; Washburn et al. 2000b; Washburn et al. 1999a; Washburn and Ferguson 2001b) or were derived from voltage-clamp recordings in dissociated SFO neurons as outlined above in *Electrophysiology*. Parameters for I_{KS} were chosen to allow burst firing (specifically burst termination) to evolve from underlying slow dynamics, as done previously in a model of pre-Bötzinger complex pacemaker neurons (Butera et al. 1999). We constrained model parameters according to *in vitro* patch clamp data from SFO neurons and searched the model's parameter space to account for the membrane potential modality and CV of both tonic and burst firing neurons. All model parameter values are given in Table 1. Simulations were performed in MATLAB (R2017a, MathWorks), where ordinary differential equations (ODEs) were solved using the forward Euler method with a time step of 0.01 ms. Standard methods of dynamic systems analyses of ODEs (see *Results, Ionic Mechanisms of Burst Firing*

and *Transition from Burst to Tonic Firing*) were performed using XPPAUT software (Ermentrout 2002).

Experimental Design & Statistical Analysis

Analyses of voltage- and current-clamp data were performed off-line using Spike2 v7 (Cambridge Electronics Design, Cambridge, UK), Signal v6 (Cambridge Electronics Design, Cambridge, UK), GraphPad Prism 6.07 (La Jolla, CA), Origin 2017 (OriginLab Corporation, USA), and MATLAB R2017a (MathWorks). Data are reported as mean ± SD. Unpaired Student's t-tests were used for statistical comparison of two unpaired groups. Standard one-way analysis of variance (ANOVA) was used for statistical comparison of multiple means. The extra sum-of-squares F test was used for statistical comparison of goodness-of-fit. The level of significance for all statistical tests was $P < 0.05$.

RESULTS

Classification of SFO neuron spiking behaviour

SFO neuron behaviour was quantified using current-clamp recordings (t = 985 s, SEM = 129 s) from 58 different SFO neurons which were analyzed to measure membrane potential distribution modality and CV of ISIs. Previous studies show that spontaneously burst firing SFO neurons exhibit depolarizing plateaus during a burst (Washburn et al. 2000b), leading to fluctuations between two membrane potential states: a hyperpolarized quiescent state (down state) and a depolarized firing state (up state). Accordingly, a neuron was classified as tonic firing if the resulting membrane potential distribution was unimodal (Figure 1C*i*, grey), or burst firing if the distribution was bimodal (ie. exhibited dual up and down states; Figure 1C*ii*, black). Consequently, 43% (n = 25/58) of SFO neurons were classified as tonic firing, and 57% (n =

33/58) were classified as burst firing, which is consistent with previous findings (Washburn et al. 2000b).

We then quantified tonic and burst firing behaviour in SFO neurons based on spike train variability. During a current-clamp recording, burst firing SFO neurons can exhibit a diversity of firing patterns, ranging from bursts to single action potentials to periods of quiescence (Washburn et al. 2000b). Therefore, we hypothesized that burst firing neurons would exhibit greater spike train variability than tonic firing neurons, testing this hypothesis by measuring the CV of ISIs. As expected, burst firing neurons had a significantly higher mean CV relative to tonic firing neurons (tonic firing: CV = 0.56 ± 0.20, n = 25; burst firing CV = 3.64 ± 1.39, n = 33; $P < 0.0001$, Student's t-test). The frequency histogram plotted for all CV values (Figure 1D) showed two distinct distributions: the first containing tonic firing neurons was best fit with a single Gaussian function (grey fit; no *P*-value), and the second containing burst firing neurons was best fit with the sum of two Gaussian functions (black fit; $F(3, 19) = 9.782$, $P = 0.0004$, $R^2 = 0.8108$, extra sum-of-squares F test), indicating the second distribution was bimodal. Therefore, burst firing SFO neurons were divided into two subpopulations, referred to as B1 and B2 neurons (B1 neurons: CV = 2.02 ± 0.35, n = 10, $1.4 < CV \leq 2.7$; B2 neurons: CV = 4.35 ± 1.01, n = 23, $CV > 2.7$). No neurons in our analysis had $0.93 < CV < 1.4$, so we defined a classification threshold (grey dashed line) half way between this range of undefined values (tonic firing: $CV < 1.16$; burst firing: $CV \geq 1.16$). Thus, membrane potential distribution modality and CV of ISIs provided a principled means to classification of tonic and burst firing behaviour in SFO neurons.

Tonic and Burst Firing Behaviour in Model

The SFO neuron model (Figure 2A; described in *Methods*) accounts for the membrane potential modality and CV of both burst and tonic firing behaviour, henceforth referred to as the

burst (Figure 2B) and tonic (Figure 2C) firing regimes, respectively. The burst firing regime exhibited membrane potential bimodality (Figure 2B*ii*) and there was no significant difference in CV relative to real burst firing SFO neurons (Figure 2B*iii*; real burst firing (black): CV = 2.02 ± 0.35, n = 10; model burst firing (red): CV = 2.00 ± 0.09, n = 10; $P = 0.79$, Student's t-test). Furthermore, by increasing the size of either I_{Na} or I_K we were able to transition from the burst to tonic firing in the model (Figure 2A*ii*). This approach resulted in two different tonic firing regimes (Figure 2C) where, relative to the burst firing regime, one had a large I_K current (tonic↑I_K; blue) and the other had a large I_{Na} (tonic↑I_{Na}; green). Both tonic↑I_K and tonic↑I_{Na} exhibited membrane potential unimodality (Figure 2C*ii*) and there was no significant difference in CV between real tonic firing, tonic↑I_K, or tonic↑I_{Na} neurons (Figure 2C*iii*; real tonic firing: CV = 0.56 ± 0.20, n = 25; tonic↑I_K: CV = 0.59 ± 0.06, n = 25; tonic↑I_{Na}: CV = 0.53 ± 0.10, n = 25; $F(2,72) = 1.29$, $P = 0.28$, one-way ANOVA).

Mechanisms of Burst Firing

We explored the mechanisms underlying the burst firing regime in our model by lowering the maximal conductance parameter, g_γ, for individual currents and measuring the subsequent effect on mean CV, membrane potential distribution modality, and resting membrane potential (RMP). Our control (Figure 3A*i*) for this analysis is the same burst firing regime shown in Figure 2B and contains all currents as presented in Equation 1 (see *Methods*).

Initiation: Burst initiation in SFO neurons has been suggested to result from depolarizing afterpotentials (DAP), which occur via activation of I_{NaP} following depolarization to the I_{NaP} threshold carried by I_{NSCC} (Fry and Ferguson 2007; Washburn et al. 2000b; Washburn et al. 1999b). In our model, burst initiation occurs for two similar reasons. First, the model contains an active I_{NSCC}, which, when blocked ($g_{NSCC} = 0$), hyperpolarizes RMP and eliminates spontaneous

firing (control: RMP = -58 mV, CV = 2.01 ± 0.07, n = 50; – I_{NSCC}: RMP = -68 mV, CV = 0, n = 50, data not shown). Secondly, burst initiation occurs via activation of I_{NaP}. Blocking only I_{NaP} (g_{NaP} = 0) results in inhibition of all spontaneous activity, but the RMP remains the same relative to control (– I_{NaP}: RMP = -58 mV, CV = 0, n = 50, data not shown). Simultaneous inhibition of I_{NSCC} and I_{NaP} are shown in Figure 3A*ii* (– I_{NSCC} – I_{NaP}: RMP = -68 mV, CV = 0, n = 50). In summary, these results show that the I_{NSCC} is required to depolarize the membrane potential to the activation range of I_{NaP} which then initializes spiking.

Maintenance: Activation of an extracellular calcium-sensing receptor (CaR) increases the length of the depolarizing plateau potentials during evoked bursts in SFO neurons (Washburn et al. 2000a; b; Washburn et al. 1999b). For the sake of simplicity, we chose not to incorporate the complex dynamics of a CaR; instead, burst maintenance relies on activation of I_{Ca}. Blocking I_{Ca} (g_{Ca} = 0) decreased burst duration where bursts manifested as membrane potential oscillations (Figure 3A*iii*). This phenomenon removed membrane potential bimodality, but CV remained above the burst firing classification threshold (CV > 1.16), despite being significantly decreased (– I_{Ca}: CV = 1.47 ± 0.09, n = 50; $P < 0.0001$, Student's t-test). This demonstrates that I_{Ca} contributes to burst firing by maintaining the prolonged up state of bursts and subsequent bimodal membrane potential distribution in our model.

Termination: Termination of the depolarized plateaus in burst firing SFO neurons occurs quickly through an unidentified intrinsic mechanism (Washburn et al. 2000b; Washburn et al. 1999b). In sensory systems, intrinsic burst firing is frequently governed by slow activation of a K^+ current (Izhikevich 2007; Krahe and Gabbiani 2004). In our SFO neuron model, we introduced I_{KS} to account for burst termination. Blocking I_{KS} (g_{KS} = 0) resulted in high frequency spiking, a significantly lower CV, and membrane potential unimodality (Figure 3A*iv*; – I_{KS}: CV

= 0.22 ± 0.002, n = 50; $P < 0.0001$, Student's t-test). These results indicate that I_{KS} is required for burst termination in our model, as demonstrated by the loss of the down state and significant decrease in CV when removed. Figure 3B summarizes these mechanisms of burst initiation, maintenance, and termination as demonstrated by our model SFO neuron.

We further analyzed the role of I_{KS} in burst termination using dynamic systems analysis (Ermentrout 2002). Specifically, we looked at the interaction between the activation gating variable of I_{KS} (m_{KS}) and voltage. In the m_{KS} vs. voltage phase plane (Figure 4A), a stable limit cycle (solid red trajectory) precedes the system's unstable equilibrium point 1 (EQ1: 0.51, -43.02) and represents one burst cycle in a noiseless environment. Starting with initial conditions at spike threshold (0.36, -54.60; Figure 4A*i*, black open circle) and moving clockwise along the limit cycle, the model begins to rapidly fire in the voltage-plane. Following each spike, the model exhibits depolarizing afterpotentials (DAPs; Figure 4A*ii*), which sum to form a plateau causing the up state of the burst. Simultaneously, the voltage trajectory moves slowly towards EQ1 as I_{KS} activates (m_{KS} increases). Sufficient activation of I_{KS} ($m_{KS} \sim 0.51$ near EQ1) eventually terminates spiking and hyperpolarizes the membrane potential below the m_{KS}-nullcline (solid black line). Following burst termination, I_{KS} begins to deactivate (m_{KS} decreases) and consequently, determines the duration of the slow after-hyperpolarization (sAHP). Sufficient deactivation of I_{KS} repolarizes the voltage back to spike threshold and the limit cycle repeats. In summary, sufficient activation and slow deactivation of I_{KS} in our model supports burst termination and the sAHP, respectively. The speed with which the model goes through the limit cycle depends on the time constant of I_{KS} activation (τ_{mKS}). Small τ_{mKS} values cause the model to cycle through quickly, whereas in our model, τ_{mKS} is on the order of seconds for a longer duration of the up state and sAHP (Butera et al. 1999). The noise current (I_{noise}) contributes to

variability in burst duration by intermittently hyperpolarizing the trajectory away from the up state of the limit cycle.

***B1 and B2 Subpopulations*:** Our earlier quantification of spike train variability in real SFO neurons revealed two distinct subpopulations of burst firing neurons, B1 and B2 neurons. To this point, our analysis supported the B1 burst firing regime. To address the second subpopulation of burst firing SFO neurons, we searched over maximal conductance (g_{KS} = 0:0.1:6 mS/cm^2) and time constant of activation (τ_{mKS} = 0:1:15s) for I_{KS} to see if we could account for the higher CV seen in B2 neurons (Figure 4B). We were able to transition our model from B1 to B2 burst firing by increasing both g_{KS} and τ_{mKS} simultaneously (white arrow), which suggests that B2 SFO neurons may have a higher density of slow-activating K^+ currents that adapt on a slower timescale than B1 neurons.

Transition from Burst to Tonic Firing

As previously mentioned, the main goal of this study was to reproduce the two prominent spiking behaviours exhibited by SFO neurons, burst and tonic firing. In agreement with previous studies (Washburn et al. 2000b), our results indicate that depolarizing plateaus occur via DAP summation, so we hypothesized that we could transition from burst to tonic firing by inhibiting our models ability to generate DAPs. We tested this hypothesis by searching parameters values of the two major currents responsible for action potential generation in SFO neurons, I_{Na} and I_K (Ferguson and Bains 1996; Washburn and Ferguson 2001a). We ran model simulations for increasing values of g_{Na} (140:2:240 mS/cm^2) and g_K (1:2:300 mS/cm^2). This range was sufficiently broad and fine-grained to see the evolution of CV as the model transitioned through different spiking regimes. The model transitioned from burst to tonic firing with increases in either g_{Na} or g_K (tonic↑I_{Na}: g_{Na} = 150 to 170 mS/cm^2; tonic↑I_K: g_K = 120 to 280 mS/cm^2; Figure

4C), or by increasing the probability of delayed-rectifier K^+ channels being open at any given voltage by decreasing the I_K activation gating exponent *p* from 4 to 2 (see Table 1, data not shown). This change in the I_K activation gating exponent *p* has been used in previous models to account for a different class of delayed-rectifier currents, Kv 3.1-3.2, (Erisir et al. 1999; Golomb et al. 2007; Tateno and Robinson 2007), which have been shown to be expressed in SFO neurons (Ono et al. 2005). Together, these results suggest that tonic firing SFO neurons express larger I_K or I_{Na} than burst firing neurons.

We investigated the effect of increased I_{Na} or I_K on model dynamics, by further analyzing the dynamics of the m_{KS} vs. voltage phase plane (Figure 4D). Increasing I_{Na} or I_K in the model produced stable limit cycles that contain only a single spike (Figure 4Dii; tonic↑I_{Na}: solid green; tonic↑I_K: solid blue), rather than a burst of spikes (Figure 4A). This change in limit cycle behaviour, and subsequent change in model spiking behaviour, results from the introduction of a fast after-hyperpolarization (fAHP) following each individual action potential. The fAHP hyperpolarizes voltage away from spiking threshold (-55 mV; open circle), thus inhibiting DAP formation and successive spike summation. Consequently, tonic↑I_{Na} and tonic↑I_K neurons do not exhibit depolarizing plateaus or up states like burst firing neurons. Importantly, I_{KS} is still active in our tonic firing regime, but now contributes to the slow spike repolarization (Figure 4D*ii*, red arrow). In summary, the change in afterpotential behaviour from depolarizing (DAPs) to hyperpolarizing (fAHPs) ultimately produces the tonic firing regime in our model.

Effect of I_{noise} on Burst Firing

As described above, I_{noise} causes variability in burst firing neurons by pushing the trajectory away from the up state of the limit cycle, therefore, allowing the model to account for variable burst durations and even single spikes. To further investigate the effect that I_{noise} has on

burst firing behaviour, we incrementally increased the standard deviation of noise (σ_{noise}) by 1 $\mu A/cm^2$ and measured mean CV ± SD (n = 50) and membrane potential distribution modality, and plotted the resulting voltage trace (Figure 5). In the noise-free model (A: $\sigma_{noise} = 0$, CV = 5.45, n = 50) the bursts progress through an entire limit cycle. With the first step increase, mean CV increases slightly relative to A (B: $\sigma_{noise} = 1\ \mu A/cm^2$, CV = 5.61 ± 0.06, n = 50), but the membrane potential distribution remains bimodal. Further increases in σ_{noise}, decrease mean CV and the model switches from two-state depolarizing plateau bursts (see traces A-D) to oscillatory bursts (see E). Furthermore, as σ_{noise} is increased, mean CV remains above burst firing classification threshold (CV ≥ 1.16, grey dashed line), but there is a shift in the membrane potential distribution from bimodal to unimodal (A: peak 2 > peak 1; B: peak 2 ≈ peak 1; C and B1 Model: to peak 2 < peak 1; D and E: only peak 1). In summary, these results indicate that as we increase I_{noise} ($0 \leq \sigma_{noise} \leq 20$) the model behaviour changes from exhibiting long, dual-state bursts to short, oscillatory bursts mixed with single action potentials.

DISCUSSION

Cellular mechanisms underlying SFO neuron spiking behaviour

We present, to the best of our knowledge, the first model of SFO neurons, that accounts for the membrane potential distribution modality and spike train variability of both tonic and burst firing SFO neurons. We confirmed that the burst firing regime requires I_{NSCC}, $I_{NaP,}$ and I_{Ca} for DAP-mediated burst initiation and maintenance, and suggest that a slow-activating K^+ current (I_{KS}) is required for burst termination and the sAHP. The model also predicts that increases in Na^+ or K^+ currents and subsequent hyperpolarization of spike afterpotential ultimately distinguishes between tonic and burst firing SFO neurons. These predictions both

confirm previously established spiking mechanisms in SFO neurons and simultaneously, lay the groundwork for future experiments to investigate unidentified ionic mechanisms that may be critical to the diversity in SFO spiking behaviour.

Burst firing, one of two major spiking behaviours exhibited by SFO neurons, has been studied in a diverse range of neuron populations using both experimental and modeling techniques. Generally, these studies have determined that this intrinsic behaviour results from a mixture of voltage- and/or calcium-dependent currents that activate and inactivate on different timescales to allow a neuron to initiate, maintain, and terminate bursts (Izhikevich 2007). One phenomenon that appears universal for burst initiation and maintenance is the generation of DAPs, though the ionic mechanism underlying its generation varies between neuron populations. For example, DAP generation in CA1 pyramidal cells and pre-Botzinger complex neurons relies on the activation of a I_{NaP} (Pace et al. 2007; Yue et al. 2005), whereas magnocellular neurosecretory cells (MNCs) primarily require changes in the intracellular Ca^{2+} concentration ($[Ca^{2+}]_i$) and the subsequent inhibition of a leak K^+ current to trigger DAPs and burst firing (Andrew 1987; Andrew and Dudek 1984; Bourque 1986; Li et al. 1995; Li and Hatton 1997). Previous patch clamp studies in intrinsically burst firing SFO neurons show that activation of a NSCC can result in DAP formation (Washburn et al. 1999b). Specifically, when NSCC is activated by a CaR, this pathway relies on G-protein activation and a change in $[Ca^{2+}]_i$. As similarly demonstrated by our model, activation of I_{NSCC} leads to a depolarization of the membrane potential to the threshold of I_{NaP}, and this initiates DAP generation and burst firing in SFO neurons (Washburn et al. 2000b).

Despite our comprehensive understanding of burst initiation and maintenance in SFO neurons, the mechanism for burst termination remains unknown. Bursts in SFO neurons typically

last 1-2 s in duration (Ferguson and Bains 1996), a length consistent with bursts in MNCs (Ohbuchi et al. 2015) and gonadotropin-releasing hormone (GnRH) neurons (Chu et al. 2012). Burst termination and the sAHP are often governed by underlying slow current dynamics including slow inactivation of an inward current or more often, slow activation of an outward K^+ current (Izhikevich 2007; Krahe and Gabbiani 2004; Larsson 2013). In this study, we show that the slow activation and deactivation of I_{KS} in our model drives burst termination and the slow repolarization to spike threshold via a sAHP. Although I_{KS} in our model is theoretical, numerous K^+-dependent mechanisms for burst termination and sAHP development have been identified in other neuron types. These mechanisms include activation of K_{Ca} currents in GnRH, Purkinje, and CA1 pyramidal neurons (Alger and Nicoll 1980; King et al. 2015; Lee et al. 2010; Liu and Herbison 2008; Swensen and Bean 2003), ATP-dependent K^+ currents in substantia nigra neurons (Knowlton et al. 2018; Schiemann et al. 2012), and M-currents in neocortical chattering neurons (Wang 1999); all of which have been shown to be expressed in SFO neurons (Hindmarch et al. 2008). Moreover, it is certainly possible that burst termination in SFO neurons results from some combination of slow-activating K^+ currents as previously found in pre-Bötzinger complex neurons (Krey et al. 2010), or a combination of K^+ currents and autocrine signalling factors as seen in vasopressin neurons (Brown and Bourque 2004; Ohbuchi et al. 2015).

The other prominent spiking behaviour in SFO neurons is tonic firing. Accordingly, we sought to transition the model from burst to tonic firing such that we could investigate the potential ionic mechanisms supporting this firing regime. In intrinsically burst firing neurons, including SFO neurons, suppression of the DAP via various current and Ca^{2+} signalling blockers has been shown to prevent bursting by inhibiting spike summation (Ghamari-Langroudi and

Bourque 1998; Ghamari-Langroudi and Bourque 2002; Li and Hatton 1997; Washburn et al. 2000b; Washburn et al. 1999b) and, in some cases, results in the neurons exclusively firing single action potentials (Ghamari-Langroudi and Bourque 2002; Yue et al. 2005). These findings suggest that it may be possible to transition an intrinsically burst firing neuron to tonic firing by inhibiting their ability to generate DAPs, while still preserving their ability to fire action potentials. Pharmacological suppression of DAPs is paralleled by our model via increases in I_K or I_{Na} and the resultant increase in fAHP size. As demonstrated by tonic↑I_{Na} and tonic↑I_K, larger fAHPs inhibit spike summation and DAP formation and, as hypothesized, this transitions the model from burst to tonic firing. Typically, the fAHP influences action potential width, duration, and frequency (Storm 1987), and is subject to modulation by various ionic conductances. In our model the fAHP is modulated directly by I_K and indirectly by I_{Na}, where the latter merely increases action potential height and strengthens the driving force of K^+ ions. In other neuron populations, such as MNC and CA1 neurons, the fAHP has been shown to be facilitated by other K^+ currents, including I_A (Bourque et al. 1998) and BK-type I_{KCa} (Storm 1987). However, Kv3-derived I_K is the dominant current underlying fAHP generation in both auditory neurons (Wang et al. 1998) and FS inhibitory cortical interneurons (Erisir et al. 1999; Golomb et al. 2007). FS interneurons have been shown to exhibit patterns of high-frequency firing as a result of their unique expression of Kv3.1-3.2 derived I_K. It is therefore unsurprising then that we were able to transition our model from burst to tonic firing by modifying the activation gating properties of I_K in our model to mimic those of Kv3.1-3.2 channels in FS interneuron models (Erisir et al. 1999; Golomb et al. 2007). Guided by our model's predictions, future *in vitro* experiments should work to identify the mechanisms underlying heterogeneity in SFO spiking behaviour and to identify the current(s) underlying burst termination in burst firing SFO neurons.

Modulation of SFO spiking behaviour

The lack of blood-brain barrier and dense expression of receptors in the SFO allows SFO neurons to sense and respond to a diverse range of signals from the peripheral circulation and cerebrospinal fluid (Hindmarch and Ferguson 2016). SFO neurons have small dendritic trees and receive the majority of their afferent input from circulating signals that bind to receptors directly on the cell body (Dellmann and Simpson 1979; Smith and Ferguson 2010). They also maintain their membrane properties and peptide responsiveness in dissociated preparations (Ferguson et al. 1997), which in combination with their unique anatomical features, reasons that SFO neurons may be one of the few neuron populations ideal to investigate using a single-compartment soma model as we have done in this study. Responses to signalling molecules manifest as changes in SFO neuron excitability through the modulation of conductance and/or the activation and inactivation properties of different ion channels. Our model demonstrates that SFO neuron spiking behaviour is dependent on a few key ionic currents, where many of these same currents that have shown to be modulated in real SFO neurons by various circulating factors. For example, the active NSCC in our model may account for the modulation of I_{NSCC} in SFO neurons by various signalling factors known to potentiate this conductance, including Ang II, interleukin 1β, glucose, ghrelin, and apelin (Dai et al. 2013; Desson and Ferguson 2003; Medeiros et al. 2012; Ono et al. 2001; Pulman et al. 2006). The I_{NSCC} has also been shown to be activated by a rise in intracellular Ca^{2+} concentration following CaR activation (Washburn et al. 2000a). Therefore, the presence and binding of these signalling molecules at the soma may initiate burst firing in SFO neurons by rapidly activating I_{NSCC} and depolarizing membrane potential to I_{NaP} threshold. Alternatively, fewer signalling factors have been identified to exert their effects on

493 SFO neurons via modulation of I_{NaP} (Fry et al. 2008; Kuksis and Ferguson 2015). Whole-cell
494 patch clamp studies have identified that I_{NaP} is the primary current underlying subthreshold
495 oscillations in SFO neurons and therefore, presumably regulates their excitability (Fry and
496 Ferguson 2007). At lower membrane potentials, the more hyperpolarized activation threshold of
497 I_{NaP} suggests it plays a larger role in influencing spike initiation than its transient counterpart.
498 Previous studies show that I_{NaP} activation threshold can be modulated by a differential expression
499 of the β subunits in voltage-gated Na^+ channels (Qu et al. 2001), although differences in I_{NaP} and
500 β subunit expression has yet to be investigated in burst and tonic firing SFO neurons. One of the
501 currents we investigated when transitioning our model to tonic firing was I_{Na}. Previous studies
502 demonstrate that long term exposure to tumor necrosis factor α (TNFα), an inflammatory
503 cytokine, potentiates I_{Na} by hyperpolarizing its activation threshold and results in an increase in
504 SFO neuron firing rate and overall excitability (Simpson and Ferguson 2017). These recent
505 findings demonstrate that different physiological states have the ability to modulate SFO channel
506 expression and/or conductance and consequently, influence SFO neuron spiking behaviour.
507 Beyond these internal membrane dynamics, SFO neurons receive some synaptic input
508 from afferent projection sites (Smith and Ferguson 2010) and is comprised of at least three
509 molecularly distinct populations of cells, including excitatory neurons, inhibitory neurons, and
510 glial cells (Oka et al. 2015), with various interconnected relationships between the three
511 populations (Hiyama and Noda 2016; Matsuda et al. 2017). In order to effectively mediate
512 communication between SFO neurons and their downstream target sites, is it reasonable to
513 assume that these various synaptic signalling pathways can influence, or potentially even
514 transition, the spiking behaviour of SFO neurons. In agreement with this, it has been previously
515 shown that antagonism of GABAergic receptors in the SFO results in burst-like discharges in

nearly half of SFO neurons (Osaka et al. 1992); a proportion consistent with our findings. Anatomical data suggests that the major source of afferent inhibitory input to the SFO extends from the MnPO and OVLT (Matsuda et al. 2017; Oka et al. 2015), and that immediately following drinking, GABAergic neurons from the MnPO activate and monosynaptically inhibit glutamatergic SFO thirst neurons (Augustine et al. 2018). Additional optogenetic analysis of SFO microcircuitry show that spontaneously active GABAergic interneurons within the SFO also modulate the activity of neighbouring glutamatergic projection neurons and, consequently, allow the SFO to differentially regulate water intake and salt appetite (Matsuda et al. 2017; Oka et al. 2015; Zimmerman et al. 2016). Together these findings suggest that tonic inhibitory drive at the SFO may direct SFO neuron spiking behaviour, and subsequently allows the SFO to differentially regulate physiologically important functions like thirst and feeding. These findings also raise questions about the molecular phenotype of burst and tonic firing SFO neurons. While beyond the scope of this paper, future studies should examine how these aforementioned circulating factors, as well as synaptic connectivity and molecular phenotype, may influence SFO neuron firing behaviour and function.

Role of burst firing in SFO

Consistent with previous studies (Washburn et al. 2000b), we found that more than half of SFO neurons analyzed exhibited burst firing. Although the functional role has yet to be elucidated in SFO neurons, it is suggested that burst firing can mediate selective communication between diverse projection sites (Izhikevich 2002) or allow for the preferential release of neuropeptides, as seen in hypothalamic neuroendocrine cells (Andrew and Dudek 1983; Bicknell and Leng 1981; Roper et al. 2004; reviewed by van den Pol 2012). SFO neurons have been shown to use the neuropeptide Ang II to communicate with the paraventricular nucleus (Li and

539 Ferguson 1993), a pathway suggested to be a major contributor to hypertension (Ferguson and
540 Renaud 1984). Ang II in the SFO has also been shown to modulate other homeostatic processes,
541 such as fluid balance (Simpson and Routtenberg 1975; 1973), salt appetite (Matsuda et al. 2017),
542 and inflammation (Benigni et al. 2010; Zubcevic et al. 2017) through distinct neuronal
543 projections. These findings suggest that the selective communication and release of physiological
544 important neuropeptides mediated by burst firing may be essential for the SFO's integration and
545 regulation of physiological function.

546 **Noise in real SFO neurons**

547 Current noise (I_{noise}) represents the effects of accumulated stochastic events occurring for
548 all ion channels in a given patch of cell membrane. In this study, I_{noise} influenced our model such
549 that large current noise ultimately decreased burst duration and increased the number of single
550 action potentials in burst firing neurons. A behaviour change like this in real SFO neurons could
551 be potentially detrimental for reliable transmission of information (Lisman 1997). The source of
552 noise in single isolated neurons derives from the finite number of ion channels in the cell
553 membrane. SFO neurons exhibit high input resistance (Ferguson and Bains 1996) implying that
554 even small changes in the proportion of open ion channels, may have a large effect on membrane
555 potential fluctuation (Johansson and Arhem 1994). Therefore, it is conceivable that I_{noise} in our
556 model is having similar effects on membrane potential to any single- or multi-channel openings
557 that may occur during a current-clamp recording. Further analysis of *in vitro* and *in vivo* noise
558 are required to determine potential roles of noise dynamics in influencing SFO neuron signaling.

559 **Toward integrative approaches to studying neuronal function**

560 The SFO has been implicated in a wide range of ANS function, including recent views
561 that it is an important site for signal integration. Emerging evidence suggests that considerable

signal integration occurs in single SFO neurons, but these findings have been mainly limited to peptides that traditionally influence the same physiological system (Smith and Ferguson 2010). Recent patch clamp studies in dissociated SFO neurons have attempted to examine the integration by single SFO neurons of Ang II and cholecystokinin, two peptides known for their traditionally different roles in cardiovascular and metabolic function (Cancelliere and Ferguson 2017). Despite these efforts, comprehensive examination of signal integration across various physiological systems represents a daunting task for plausible experimental design. Recent studies have provided a window into the neural circuitry through which different populations of SFO neurons selectively influence thirst and salt appetite (Hiyama and Noda 2016; Matsuda et al. 2017; Zimmerman et al. 2017). These studies represent a step towards understanding how the SFO selectively influences physiological function, and they begin to address signal integration across physiological systems that have traditionally been viewed as separate. Interestingly, there is an emerging body of literature suggesting the SFO may be integrating pro-inflammatory signals (ie. TNFα or IL-1β) with cardiovascular signals (ie. Ang II) to upregulate the RAS system and potentiate Ang II-induced hypertension at the SFO (Wei et al. 2015; Yao et al. 2017; Zhang et al. 2014), but the neuronal mechanisms underlying this phenomenon have only recently begun to be investigated (Simpson and Ferguson 2017; 2018). The goal in the development of our SFO neuron model is to expedite such investigations by offering mechanistic explanations for experimental data and providing testable predictions about the integration of signals, like TNFα and Ang II, at the SFO. One of the greatest strengths of single neuron models is their ability to be parameterized by and integrated with experimental studies, thus creating a virtuous and efficient cycle for the study of neuron behaviour. Combination modeling and electrophysiology studies have been used to study a wide range of neuronal function across the

585 CNS (Erisir et al. 1999; Feetham et al. 2015; Golomb et al. 2007; Klaus et al. 2011; MacGregor
586 and Leng 2013; Roper et al. 2004; Roper et al. 2003).

587 **Conclusions**

588 We present, to the best of our knowledge, the first ever model of SFO neurons. Through
589 *in vitro* patch clamp data and quantitative classification of SFO neuron spiking behaviour, we
590 constrained our model by stipulating it must account for the membrane potential distribution and
591 spike train variability of tonic and burst firing SFO neurons. The model predicts that
592 heterogeneity in current expression and subsequent influence on spike afterpotentials underlie
593 behavioural differences between tonic and burst firing neurons, and that burst firing SFO neurons
594 have unidentified underlying slow dynamics that are required for burst termination. These
595 predictions provide a series of working hypotheses and lay the groundwork for future
596 experiments to further identify the ionic mechanisms underlying diversity in SFO firing
597 behaviour. Furthermore, future use of this model in combination with *in vitro* methodologies
598 provides us with a platform for studying the mechanisms underlying signal integration within the
599 SFO.

600

601

602

603

604

605

606

607

608

609

REFERENCES

Alger BE, and Nicoll RA. Epileptiform burst afterhyperolarization: calcium-dependent potassium potential in hippocampal CA1 pyramidal cells. *Science* 210: 1122-1124, 1980.

Anderson JW, Smith PM, and Ferguson AV. Subfornical organ neurons projecting to paraventricular nucleus: whole-cell properties. *Brain Res* 921: 78-85, 2001.

Anderson JW, Washburn DL, and Ferguson AV. Intrinsic osmosensitivity of subfornical organ neurons. *Neuroscience* 100: 539-547, 2000.

Andrew RD. Endogenous Bursting by Rat Supraoptic Neuroendocrine Cells Is Calcium Dependent. *Journal of Physiology-London* 384: 451-465, 1987.

Andrew RD, and Dudek FE. Analysis of intracellularly recorded phasic bursting by mammalian neuroendocrine cells. *J Neurophysiol* 51: 552-566, 1984.

Andrew RD, and Dudek FE. Burst discharge in mammalian neuroendocrine cells involves an intrinsic regenerative mechanism. *Science* 221: 1050-1052, 1983.

Augustine V, Gokce SK, Lee S, Wang B, Davidson TJ, Reimann F, Gribble F, Deisseroth K, Lois C, and Oka Y. Hierarchical neural architecture underlying thirst regulation. *Nature* 555: 204-209, 2018.

Benigni A, Cassis P, and Remuzzi G. Angiotensin II revisited: new roles in inflammation, immunology and aging. *EMBO Mol Med* 2: 247-257, 2010.

Bicknell RJ, and Leng G. Relative efficiency of neural firing patterns for vasopressin release in vitro. *Neuroendocrinology* 33: 295-299, 1981.

Bourque CW. Calcium-dependent spike after-current induces burst firing in magnocellular neurosecretory cells. *Neurosci Lett* 70: 204-209, 1986.

Bourque CW, Kirkpatrick K, and Jarvis CR. Extrinsic modulation of spike afterpotentials in rat hypothalamoneurohypophysial neurons. *Cell Mol Neurobiol* 18: 3-12, 1998.

Brown CH, and Bourque CW. Autocrine feedback inhibition of plateau potentials terminates phasic bursts in magnocellular neurosecretory cells of the rat supraoptic nucleus. *J Physiol* 557: 949-960, 2004.

Butera RJ, Jr., Rinzel J, and Smith JC. Models of respiratory rhythm generation in the pre-Botzinger complex. I. Bursting pacemaker neurons. *J Neurophysiol* 82: 382-397, 1999.

Cancelliere NM, and Ferguson AV. Subfornical organ neurons integrate cardiovascular and metabolic signals. *Am J Physiol Regul Integr Comp Physiol* 312: R253-R262, 2017.

Chu Z, Tomaiuolo M, Bertram R, and Moenter SM. Two types of burst firing in gonadotrophin-releasing hormone neurones. *J Neuroendocrinol* 24: 1065-1077, 2012.

Dai L, Smith PM, Kuksis M, and Ferguson AV. Apelin acts in the subfornical organ to influence neuronal excitability and cardiovascular function. *J Physiol* 591: 3421-3432, 2013.

Dellmann HD, and Simpson JB. The subfornical organ. *Int Rev Cytol* 58: 333-421, 1979.

Desson SE, and Ferguson AV. Interleukin 1beta modulates rat subfornical organ neurons as a result of activation of a non-selective cationic conductance. *J Physiol* 550: 113-122, 2003.

Erisir A, Lau D, Rudy B, and Leonard CS. Function of specific K(+) channels in sustained high-frequency firing of fast-spiking neocortical interneurons. *J Neurophysiol* 82: 2476-2489, 1999.

Ermentrout B. *Simulating, Analyzing, and Animating Dynamical Systems: A Guide to XPPAUT for Researchers and Students*. Pennsylvania, USA: SIAM, 2002.

Feetham CH, Nunn N, Lewis R, Dart C, and Barrett-Jolley R. TRPV4 and K(Ca) ion channels functionally couple as osmosensors in the paraventricular nucleus. *Brit J Pharmacol* 172: 1753-1768, 2015.

Ferguson AV, and Bains JS. Electrophysiology of the circumventricular organs. *Front Neuroendocrinol* 17: 440-475, 1996.

Ferguson AV, Bicknell RJ, Carew MA, and Mason WT. Dissociated adult rat subfornical organ neurons maintain membrane properties and angiotensin responsiveness for up to 6 days. *Neuroendocrinology* 66: 409-415, 1997.

Ferguson AV, and Li Z. Whole cell patch recordings from forebrain slices demonstrate angiotensin II inhibits potassium currents in subfornical organ neurons. *Regul Pept* 66: 55-58, 1996.

Ferguson AV, and Renaud LP. Hypothalamic paraventricular nucleus lesions decrease pressor responses to subfornical organ stimulation. *Brain Res* 305: 361-364, 1984.

Fry M, Cottrell GT, and Ferguson AV. Prokineticin 2 influences subfornical organ neurons through regulation of MAP kinase and the modulation of sodium channels. *Am J Physiol Regul Integr Comp Physiol* 295: R848-856, 2008.

Fry M, and Ferguson AV. Subthreshold oscillations of membrane potential of rat subfornical organ neurons. *Neuroreport* 18: 1389-1393, 2007.

Ghamari-Langroudi M, and Bourque CW. Caesium blocks depolarizing after-potentials and phasic firing in rat supraoptic neurones. *J Physiol (Lond)* 510 (Pt 1): 165-175, 1998.

Ghamari-Langroudi M, and Bourque CW. Flufenamic acid blocks depolarizing afterpotentials and phasic firing in rat supraoptic neurones. *J Physiol* 545: 537-542, 2002.

Golomb D, Donner K, Shacham L, Shlosberg D, Amitai Y, and Hansel D. Mechanisms of firing patterns in fast-spiking cortical interneurons. *PLoS Comput Biol* 3: e156, 2007.

Hattori Y, Kasai M, Uesugi S, Kawata M, and Yamashita H. Atrial natriuretic polypeptide depresses angiotensin II induced excitation of neurons in the rat subfornical organ in vitro. *Brain Res* 443: 355-359, 1988.

Hindmarch C, Fry M, Yao ST, Smith PM, Murphy D, and Ferguson AV. Microarray analysis of the transcriptome of the subfornical organ in the rat: regulation by fluid and food deprivation. *Am J Physiol Regul Integr Comp Physiol* 295: R1914-1920, 2008.

Hindmarch CC, and Ferguson AV. Physiological roles for the subfornical organ: a dynamic transcriptome shaped by autonomic state. *J Physiol* 594: 1581-1589, 2016.

Hiyama TY, and Noda M. Sodium sensing in the subfornical organ and body-fluid homeostasis. *Neurosci Res* 113: 1-11, 2016.

687 **Hodgkin AL, and Huxley AF**. A quantitative description of membrane current and its
688 application to conduction and excitation in nerve. *J Physiol* 117: 500-544, 1952.

689 **Holt GR, Softky WR, Koch C, and Douglas RJ**. Comparison of discharge variability in vitro
690 and in vivo in cat visual cortex neurons. *J Neurophysiol* 75: 1806-1814, 1996.

691 **Izhikevich EM**. *Dynamical Systems in Neuroscience: The Geometry of Excitability and*
692 *Bursting.* Cambridge, Massachusetts: The MIT Press, 2007, p. 441.

693 **Izhikevich EM**. Resonance and selective communication via bursts in neurons having
694 subthreshold oscillations. *Biosystems* 67: 95-102, 2002.

695 **Johansson S, and Arhem P**. Single-channel currents trigger action potentials in small cultured
696 hippocampal neurons. *Proc Natl Acad Sci U S A* 91: 1761-1765, 1994.

697 **Kinard TA, de Vries G, Sherman A, and Satin LS**. Modulation of the bursting properties of
698 single mouse pancreatic beta-cells by artificial conductances. *Biophys J* 76: 1423-1435, 1999.

699 **King B, Rizwan AP, Asmara H, Heath NC, Engbers JD, Dykstra S, Bartoletti TM, Hameed**
700 **S, Zamponi GW, and Turner RW**. IKCa channels are a critical determinant of the slow AHP
701 in CA1 pyramidal neurons. *Cell Rep* 11: 175-182, 2015.

702 **Klaus A, Planert H, Hjorth JJ, Berke JD, Silberberg G, and Kotaleski JH**. Striatal fast-
703 spiking interneurons: from firing patterns to postsynaptic impact. *Front Syst Neurosci* 5: 57,
704 2011.

705 **Knowlton C, Kutterer S, Roeper J, and Canavier CC**. Calcium dynamics control K-ATP
706 channel-mediated bursting in substantia nigra dopamine neurons: a combined experimental and
707 modeling study. *J Neurophysiol* 119: 84-95, 2018.

708 **Krahe R, and Gabbiani F**. Burst firing in sensory systems. *Nat Rev Neurosci* 5: 13-23, 2004.

709 **Krey RA, Goodreau AM, Arnold TB, and Del Negro CA**. Outward Currents Contributing to
710 Inspiratory Burst Termination in preBotzinger Complex Neurons of Neonatal Mice Studied in
711 Vitro. *Front Neural Circuits* 4: 124, 2010.

712 **Kuksis M, and Ferguson AV**. Actions of a hydrogen sulfide donor (NaHS) on transient sodium,
713 persistent sodium, and voltage-gated calcium currents in neurons of the subfornical organ. *J*
714 *Neurophysiol* 114: 1641-1651, 2015.

715 **Larsson HP**. What determines the kinetics of the slow afterhyperpolarization (sAHP) in
716 neurons? *Biophys J* 104: 281-283, 2013.

717 **Lee K, Duan W, Sneyd J, and Herbison AE**. Two slow calcium-activated
718 afterhyperpolarization currents control burst firing dynamics in gonadotropin-releasing hormone
719 neurons. *J Neurosci* 30: 6214-6224, 2010.

720 **Li Z, Decavel C, and Hatton GI**. Calbindin-D_{28k}: role in determining intrinsically generated
721 firing patterns in rat supraoptic neurones. *J Physiol (Lond)* 448 (Pt.3): 601-608, 1995.

722 **Li Z, and Ferguson AV**. Subfornical organ efferents to paraventricular nucleus utilize
723 angiotensin as a neurotransmitter. *Am J Physiol* 265: R302-309, 1993.

724 **Li Z, and Hatton GI**. Ca^{2+} release from internal stores: role in generating depolarizing after-
725 potentials in rat supraoptic neurones. *J Physiol (Lond)* 498: 339-350, 1997.

Lisman JE. Bursts as a unit of neural information: making unreliable synapses reliable. *Trends Neurosci* 20: 38-43, 1997.

Liu X, and Herbison AE. Small-conductance calcium-activated potassium channels control excitability and firing dynamics in gonadotropin-releasing hormone (GnRH) neurons. *Endocrinology* 149: 3598-3604, 2008.

MacGregor DJ, and Leng G. Spike triggered hormone secretion in vasopressin cells; a model investigation of mechanism and heterogeneous population function. *PLoS Comput Biol* 9: e1003187, 2013.

Matsuda T, Hiyama TY, Niimura F, Matsusaka T, Fukamizu A, Kobayashi K, Kobayashi K, and Noda M. Distinct neural mechanisms for the control of thirst and salt appetite in the subfornical organ. *Nat Neurosci* 20: 230-241, 2017.

McKinley MJ, Allen AM, Burns P, Colvill LM, and Oldfield BJ. Interaction of circulating hormones with the brain: the roles of the subfornical organ and the organum vasculosum of the lamina terminalis. *Clin Exp Pharmacol Physiol Suppl* 25: S61-67, 1998.

Medeiros N, Dai L, and Ferguson AV. Glucose-responsive neurons in the subfornical organ of the rat--a novel site for direct CNS monitoring of circulating glucose. *Neuroscience* 201: 157-165, 2012.

Ohbuchi T, Haam J, and Tasker JG. Regulation of Neuronal Activity in Hypothalamic Vasopressin Neurons. *Interdiscip Inf Sci* 21: 225-234, 2015.

Oka Y, Ye M, and Zuker CS. Thirst driving and suppressing signals encoded by distinct neural populations in the brain. *Nature* 520: 349-352, 2015.

Ono K, Honda E, and Inenaga K. Angiotensin II induces inward currents in subfornical organ neurones of rats. *J Neuroendocrinol* 13: 517-523, 2001.

Ono K, Toyono T, Honda E, and Inenaga K. Transient outward K+ currents in rat dissociated subfornical organ neurones and angiotensin II effects. *J Physiol* 568: 979-991, 2005.

Osaka T, Yamashita H, and Koizumi K. Inhibitory inputs to the subfornical organ from the AV3V: involvement of GABA. *Brain Res Bull* 29: 581-587, 1992.

Pace RW, Mackay DD, Feldman JL, and Del Negro CA. Role of persistent sodium current in mouse preBotzinger Complex neurons and respiratory rhythm generation. *J Physiol* 580: 485-496, 2007.

Pulman KJ, Fry WM, Cottrell GT, and Ferguson AV. The subfornical organ: a central target for circulating feeding signals. *J Neurosci* 26: 2022-2030, 2006.

Qu Y, Curtis R, Lawson D, Gilbride K, Ge P, DiStefano PS, Silos-Santiago I, Catterall WA, and Scheuer T. Differential modulation of sodium channel gating and persistent sodium currents by the beta1, beta2, and beta3 subunits. *Mol Cell Neurosci* 18: 570-580, 2001.

Roper P, Callaway J, and Armstrong W. Burst initiation and termination in phasic vasopressin cells of the rat supraoptic nucleus: a combined mathematical, electrical, and calcium fluorescence study. *J Neurosci* 24: 4818-4831, 2004.

Roper P, Callaway J, Shevchenko T, Teruyama R, and Armstrong W. AHP's, HAP's and DAP's: How potassium currents regulate the excitability of rat supraoptic neurones. *Journal of Computational Neuroscience* 15: 367-389, 2003.

Schiemann J, Schlaudraff F, Klose V, Bingmer M, Seino S, Magill PJ, Zaghloul KA, Schneider G, Liss B, and Roeper J. K-ATP channels in dopamine substantia nigra neurons control bursting and novelty-induced exploration. *Nat Neurosci* 15: 1272-1280, 2012.

Sheroziya MG, von Bohlen Und Halbach O, Unsicker K, and Egorov AV. Spontaneous bursting activity in the developing entorhinal cortex. *J Neurosci* 29: 12131-12144, 2009.

Shute L, Lee S, and Fry M. The effects of neuropeptide Y on dissociated subfornical organ neurons. In: *10th Annual Canadian Neuroscience Meeting*. Toronto, ON Canada: 2016.

Simpson JB, and Routtenberg A. Subfornical organ lesions reduce intravenous angiotensin-induced drinking. *Brain Res* 88: 154-161, 1975.

Simpson JB, and Routtenberg A. Subfornical organ: site of drinking elicitation by angiotensin II. *Science* 181: 1172-1175, 1973.

Simpson NJ, and Ferguson AV. The proinflammatory cytokine tumor necrosis factor-alpha excites subfornical organ neurons. *J Neurophysiol* 118: 1532-1541, 2017.

Simpson NJ, and Ferguson AV. Tumor necrosis factor alpha potentiates the effects of angiotensin II on subfornical organ neurons. *Am J Physiol Regul Integr Comp Physiol* 2018.

Smith PM, and Ferguson AV. Circulating signals as critical regulators of autonomic state--central roles for the subfornical organ. *Am J Physiol Regul Integr Comp Physiol* 299: R405-415, 2010.

Storm JF. Action potential repolarization and a fast after-hyperpolarization in rat hippocampal pyramidal cells. *J Physiol* 385: 733-759, 1987.

Swensen AM, and Bean BP. Ionic mechanisms of burst firing in dissociated Purkinje neurons. *J Neurosci* 23: 9650-9663, 2003.

Tanaka J, Miyakubo H, Okumura T, Sakamaki K, and Hayashi Y. Estrogen decreases the responsiveness of subfornical organ neurons projecting to the hypothalamic paraventricular nucleus to angiotensin II in female rats. *Neurosci Lett* 307: 155-158, 2001.

Tateno T, and Robinson HP. Quantifying noise-induced stability of a cortical fast-spiking cell model with Kv3-channel-like current. *Biosystems* 89: 110-116, 2007.

van den Pol AN. Neuropeptide transmission in brain circuits. *Neuron* 76: 98-115, 2012.

Wang LY, Gan L, Forsythe ID, and Kaczmarek LK. Contribution of the Kv3.1 potassium channel to high-frequency firing in mouse auditory neurones. *J Physiol* 509 (Pt 1): 183-194, 1998.

Wang XJ. Fast burst firing and short-term synaptic plasticity: a model of neocortical chattering neurons. *Neuroscience* 89: 347-362, 1999.

Washburn DL, Anderson JW, and Ferguson AV. The calcium receptor modulates the hyperpolarization-activated current in subfornical organ neurons. *Neuroreport* 11: 3231-3235, 2000a.

Washburn DL, Anderson JW, and Ferguson AV. A subthreshold persistent sodium current mediates bursting in rat subfornical organ neurones. *J Physiol* 529 (Pt 2): 359-371, 2000b.

Washburn DL, Beedle AM, and Ferguson AV. Inhibition of subfornical organ neuronal potassium channels by vasopressin. *Neuroscience* 93: 349-359, 1999a.

Washburn DL, and Ferguson AV. Membrane properties of subfornical organ neutrons. *Clin Exp Pharmacol Physiol* 28: 575-580, 2001a.

Washburn DL, and Ferguson AV. Selective potentiation of N-type calcium channels by angiotensin II in rat subfornical organ neurones. *J Physiol* 536: 667-675, 2001b.

Washburn DL, Smith PM, and Ferguson AV. Control of neuronal excitability by an ion-sensing receptor (correction of anion-sensing). *Eur J Neurosci* 11: 1947-1954, 1999b.

Wei SG, Yu Y, Zhang ZH, and Felder RB. Proinflammatory cytokines upregulate sympathoexcitatory mechanisms in the subfornical organ of the rat. *Hypertension* 65: 1126-1133, 2015.

Yang F, Zhou L, Wang D, Yang LL, Yuan GR, and Huang QY. Suppression of TRPV4 channels ameliorates anti-dipsogenic effects under hypoxia in the subfornical organ of rats. *Sci Rep* 6: 30168, 2016.

Yao ST, McKinley MJ, and May CN. Circumventing a broken heart: cytokines and the subfornical organ. *Am J Physiol Heart Circ Physiol* 313: H729-H731, 2017.

Yue C, Remy S, Su H, Beck H, and Yaari Y. Proximal persistent Na+ channels drive spike afterdepolarizations and associated bursting in adult CA1 pyramidal cells. *J Neurosci* 25: 9704-9720, 2005.

Zhang J, Patel MB, Griffiths R, Mao A, Song YS, Karlovich NS, Sparks MA, Jin H, Wu M, Lin EE, and Crowley SD. Tumor necrosis factor-alpha produced in the kidney contributes to angiotensin II-dependent hypertension. *Hypertension* 64: 1275-1281, 2014.

Zimmerman CA, Leib DE, and Knight ZA. Neural circuits underlying thirst and fluid homeostasis. *Nat Rev Neurosci* 18: 459-469, 2017.

Zimmerman CA, Lin YC, Leib DE, Guo L, Huey EL, Daly GE, Chen Y, and Knight ZA. Thirst neurons anticipate the homeostatic consequences of eating and drinking. *Nature* 537: 680-684, 2016.

Zubcevic J, Santisteban MM, Perez PD, Arocha R, Hiller H, Malphurs WL, Colon-Perez LM, Sharma RK, de Kloet A, Krause EG, Febo M, and Raizada MK. A Single Angiotensin II Hypertensive Stimulus Is Associated with Prolonged Neuronal and Immune System Activation in Wistar-Kyoto Rats. *Front Physiol* 8: 592, 2017.

FIGURE CAPTIONS

Figure 1. Classification of SFO neurons based on membrane potential distribution and spike train variability. *A-B:* Representative tonic (A, grey) or burst (B, black) firing behaviour in two different SFO neurons. *C:* Histograms show the membrane potential distribution of the tonic (*i*, grey) and burst (*ii*, black) firing SFO neuron from A and B, respectively. Bin width is 0.3 mV. 43% (n = 25/58) of neurons were classified as tonic firing and 57% (n = 33/58) were classified as burst firing based on modality. *D:* Histogram shows the distribution of CV across all analyzed SFO neurons (n = 58, bin width = 0.3). CV distribution for tonic firing neurons was best fit with a single Gaussian function (no *P*-value; grey), whereas the CV distribution for burst firing neurons was best fit with the sum of two Gaussian functions ($F(3, 19) = 9.782$, $P = 0.0004$, $R^2 = 0.81$; black). As a result, burst firing SFO neurons were further divided into B1 and B2 subpopulations (B1: CV = 2.02 ± 0.35, n = 10, $1.4 < CV \leq 2.7$; B2: CV = 4.35 ± 1.01, n = 23, $CV > 2.7$). Vertical grey dashed line represents the classification threshold for neuron spiking behaviour (tonic firing: $CV < 1.16$; burst firing: $CV \geq 1.16$).

Figure 2. Burst and tonic firing behaviour in SFO neuron model. *A:* Hodgkin-Huxley type model of SFO neurons. (i) Equivalent circuit diagram. Arrow across the resistor indicates a voltage-dependent current, no arrow indicates a linear current. (ii) Model transitions from burst to tonic firing by increasing the transient Na^+ current (I_{Na}; green arrow) or delayed-rectifier K^+ current (I_K; blue arrow). *B:* Burst firing regime in the model SFO neuron. (i) An *in vitro* recording from (black) and model of (red) a burst firing SFO neuron. Box shows individual burst. (ii) Histogram (red) showing the membrane potential bimodality of the model trace in *Bi*. Bin width is 0.5 mV. (iii) No significant difference between mean CV of real and model burst firing SFO neurons (real: CV = 2.02 ± 0.35, n = 10; model: CV = 2.00 ± 0.09, n = 10; $P = 0.79$;

student's t-test). *C:* Tonic firing regime in model SFO neuron. (i) An *in vitro* recording from (black) and model of (blue, green) tonic firing SFO neurons. The model transitions from burst to tonic firing by increasing I_K (tonic↑I_K; blue trace) or I_{Na} (tonic↑I_{Na}; green trace). (ii) Histograms show the membrane potential unimodality of the models in *Ci*. Bin width is 0.5 mV. (iii) There was no significant difference between mean CV values of real tonic firing, tonic↑I_K, or tonic↑I_{Na} neurons (real tonic firing: CV = 0.56 ± 0.20, n = 25; tonic↑I_K: CV = 0.59 ± 0.06, n = 25; tonic↑I_{Na}: CV = 0.53 ± 0.10, n = 25; F(2,72) = 1.29, P = 0.28; one-way ANOVA). Scale bars for voltage traces: burst firing = 5 s x 10 mV, tonic firing = 1 s x 10 mV.

Figure 3. Burst initiation, maintenance and termination in SFO neuron model. *A*: The effect of inhibiting individual model currents on CV of ISIs, membrane potential (MP) distribution modality, and resting membrane potential (RMP). (i) Burst firing regime as shown in Figure 2 (control: CV = 2.01 ± 0.07, n = 50, RMP = -58 mV, bimodal MP distribution). (ii) *Initiation:* Blocking I_{NSCC} and I_{NaP} in the model (g_{NSCC} = 0, g_{NaP} = 0; $-I_{NSCC}$ and I_{NaP}: CV = 0, n = 50, no *P*-value; RMP = -68 mV; unimodal MP distribution). (iii) *Maintenance:* Blocking I_{Ca} in our model (g_{Ca} = 0; $-I_{Ca}$: CV = 1.47 ± 0.09, n = 50, $P < 0.0001$, student's t-test; RMP = -57 mV; unimodal MP distribution). (iv) *Termination:* Blocking I_{KS} in our model (g_{KS} = 0; $-I_{KS}$: CV = 0.22 ± 0.002, n = 50, $P < 0.0001$, student's t-test; RMP = -53 mV; unimodal MP distribution). *B*: Summary of mechanism underlying burst initiation (I_{NSCC}, I_{NaP}), maintenance (I_{Ca}), and termination (I_{KS}) as proposed by our model SFO neuron in *A*.

Figure 4. Membrane dynamics supporting burst and tonic firing phenotypes. *A-B*: Role of I_{KS} in modulation of burst firing behaviour. *A*: (i) Membrane dynamics in slow K^+ current activation variable (m_{KS}) vs. membrane potential (voltage) phase plane. Dotted red and solid black lines are the voltage ($dV_m/dt = 0$) and m_{KS} ($dm_{KS}/dt = 0$) nullclines, respectively. Limit

cycle (solid red) shows the orbit of a single burst. Nullclines intersect at unstable equilibrium point 1 (EQ1: 0.51, -43.02 mV; black square). Intersection of limit cycle and m_{KS}-nullcline is the spiking threshold (0.36, -54.60 mV; open black circle). Arrows indicate direction of slow (red) and fast (black) trajectory movement. Thin vertical lines represent the direction field. (ii) Enlarged phase space near spiking threshold. DAPs: Depolarizing afterpotentials. sAHP: Slow after-hyperpolarization. *B*: Search space for activation time constant (τ_{mKS}) vs maximal conductance (g_{KS}) of our slowly-activating K^+ current (I_{KS}). Greyscale indicates CV value. White arrow depicts transition between B1 and B2 burst firing. *C-D:* Transition from burst to tonic firing in our model. *C:* Increasing the size of either I_{Na} (tonic↑I_{Na}, green) or I_K (tonic↑I_K, blue) transitioned our model from burst (B, red) to tonic firing. Greyscale indicates CV value. *D:* (i) The m_{KS} vs. voltage phase plane (as introduced in A) for the tonic firing regime. Dotted green and blue lines are the m_{KS} ($dm_{KS}/dt = 0$) nullclines for tonic↑I_{Na} and tonic↑I_K, respectively. Unstable equilibrium points for tonic↑I_{Na} and tonic↑I_K are labelled EQ1 (0.51, -43.02 mV) and EQ2 (0.35, -55.40 mV), respectively. Limit cycles for tonic↑I_{Na} (solid green) and tonic↑I_K (solid blue) contain only a single spike. fAHP: Fast after-hyperpolarization. (ii) Inset shows enlarged limit cycles for tonic↑I_{Na} and tonic↑I_K, spike threshold (0.36, -54.60 mV; open black circle), and directions of fast (black arrows) and slow (red arrow) trajectory movement.

Figure 5. The effect of I_{noise} on burst firing behaviour. Models A-E have increasing standard deviations of noise (σ_{noise}, $\mu A/cm^2$). Mean CV of ISIs (CV ± SD, n = 50), voltage trace, and membrane potential (MP) distribution are plotted for each model (t = 4 min traces). Model A is noiseless ($\sigma_{noise} = 0$). Grey horizontal dashed line represents the classification threshold as previous shown in Figure 1D.

Table 1. Summary of experimentally derived parameters for the SFO neuron model.

Parameters E_{ion}, g_{γ}, *p, q, Ø, k*, and τ are explained in Methods under *Model Equations.*

* indicates parameters are further described in the results section as changes in these values lead to different firing behaviours in the model.

Table 1. Experimentally derived parameter values for the SFO neuron model.

Current	E_{ion} (mV)	g_γ (mS/cm^2)	p	q	$Ø_m$ (mV)	k_m	$Ø_h$ (mV)	k_h	τ_m (ms)	τ_h (ms)
I_{Na}	107	*	3	1	-31	6.1	-62	-6.2	0.1	0.8
I_{NaP}	107	0.13	3	1	-55	4	-45	-6	5	50
I_K	-88	*	4*	0	2	8	-	-	$7.2 - \frac{6.4}{1+e^{\frac{V+28.3}{-19.2}}}$	-
I_A	-88	3	3	1	-44	18	-60	-8	5	30
I_{Ca}	120	0.3	2	0	-14	5.8	-	-	10	-
I_{KS}	-88	3*	3	1	-44	18	-60	-8	*	10
I_{NSCC}	-35	0.2	0	0	-	-	-	-	-	-
I_L	-65	0.3183	0	0	-	-	-	-	-	-

Figure 1.

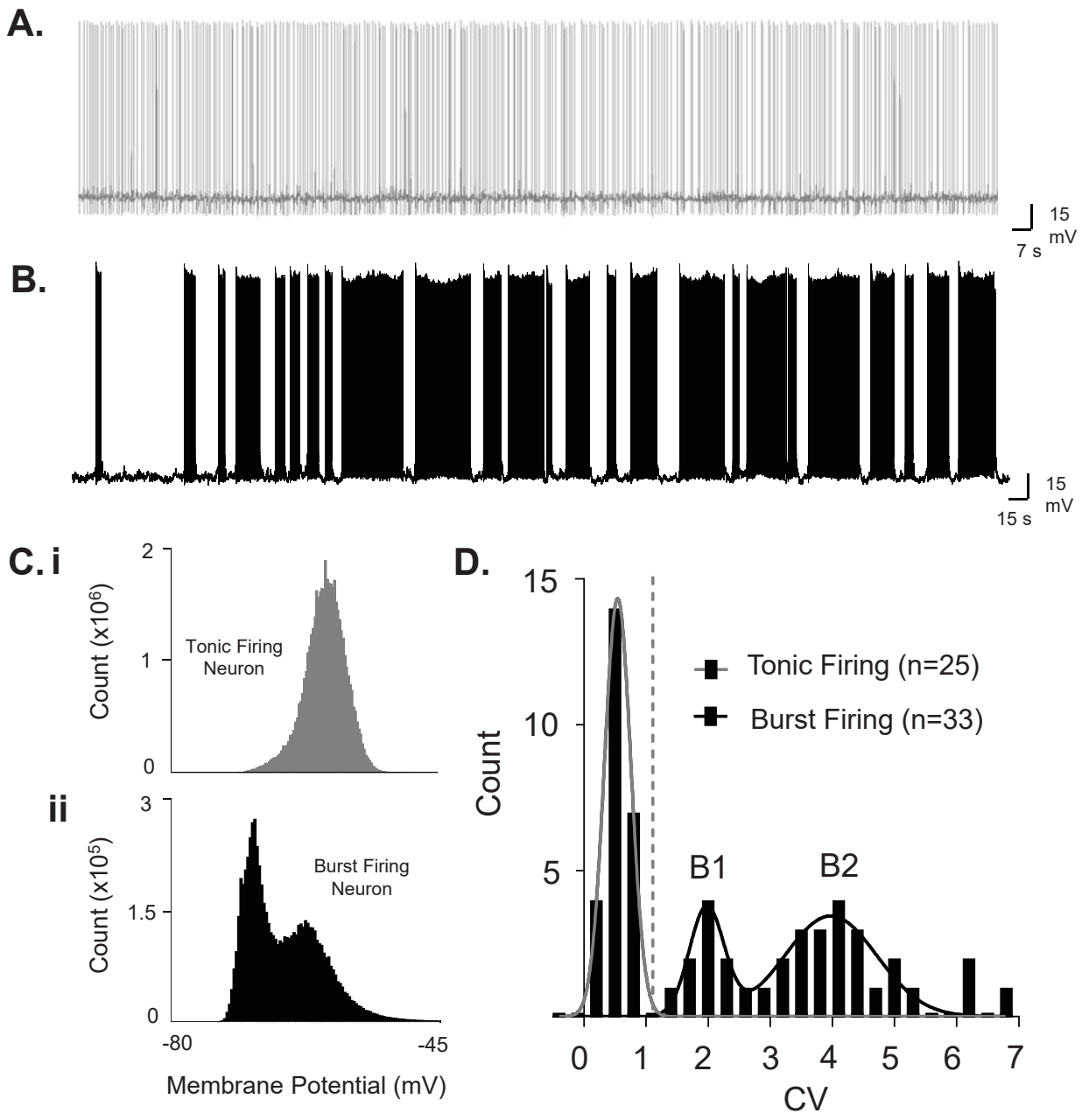

Figure 2.

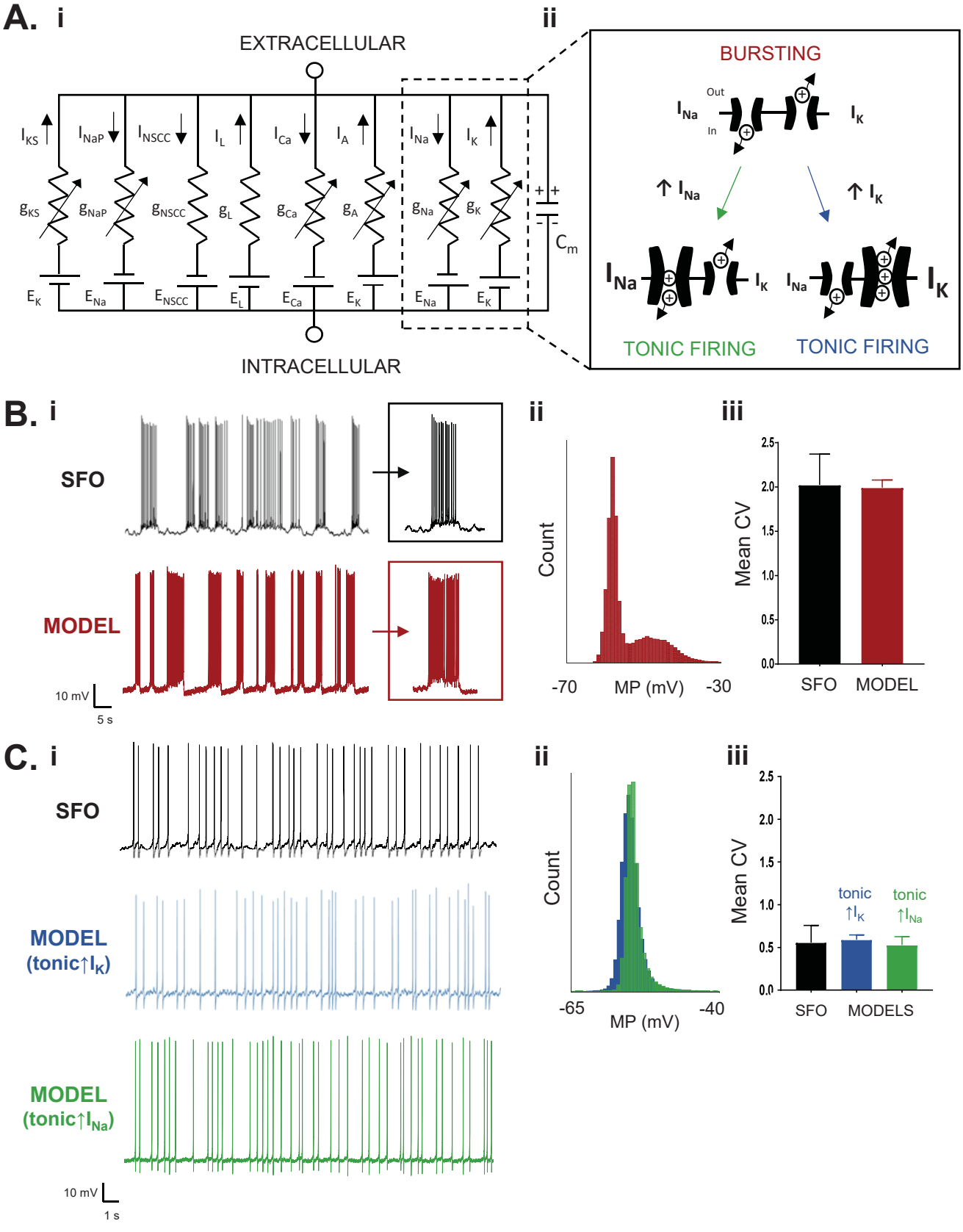

Figure 3.

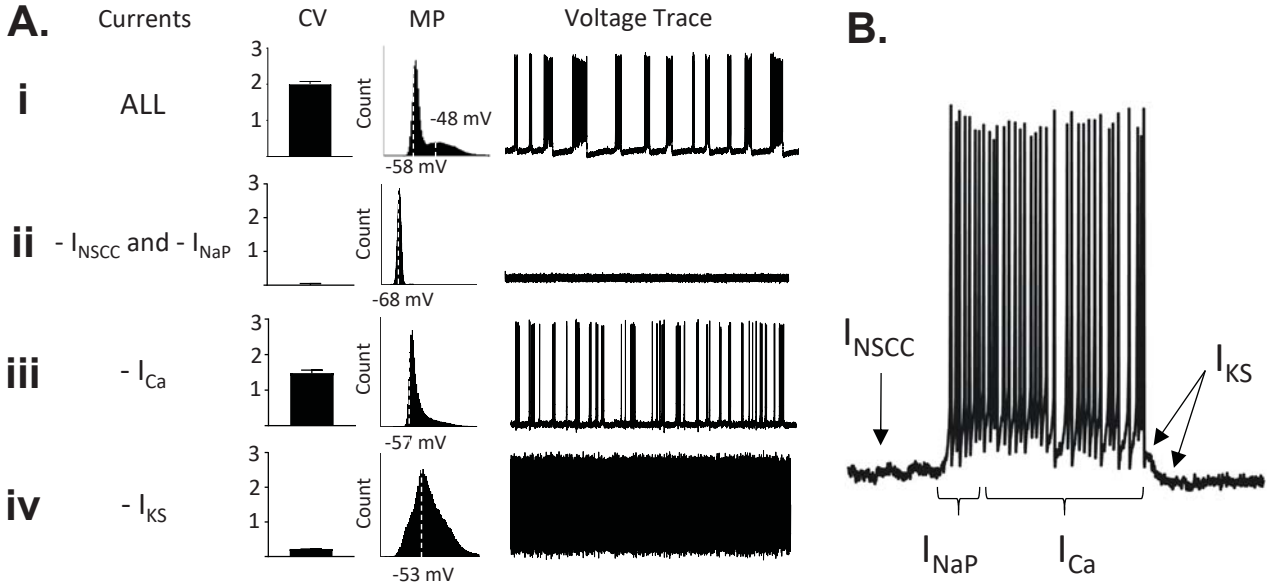

Figure 4.

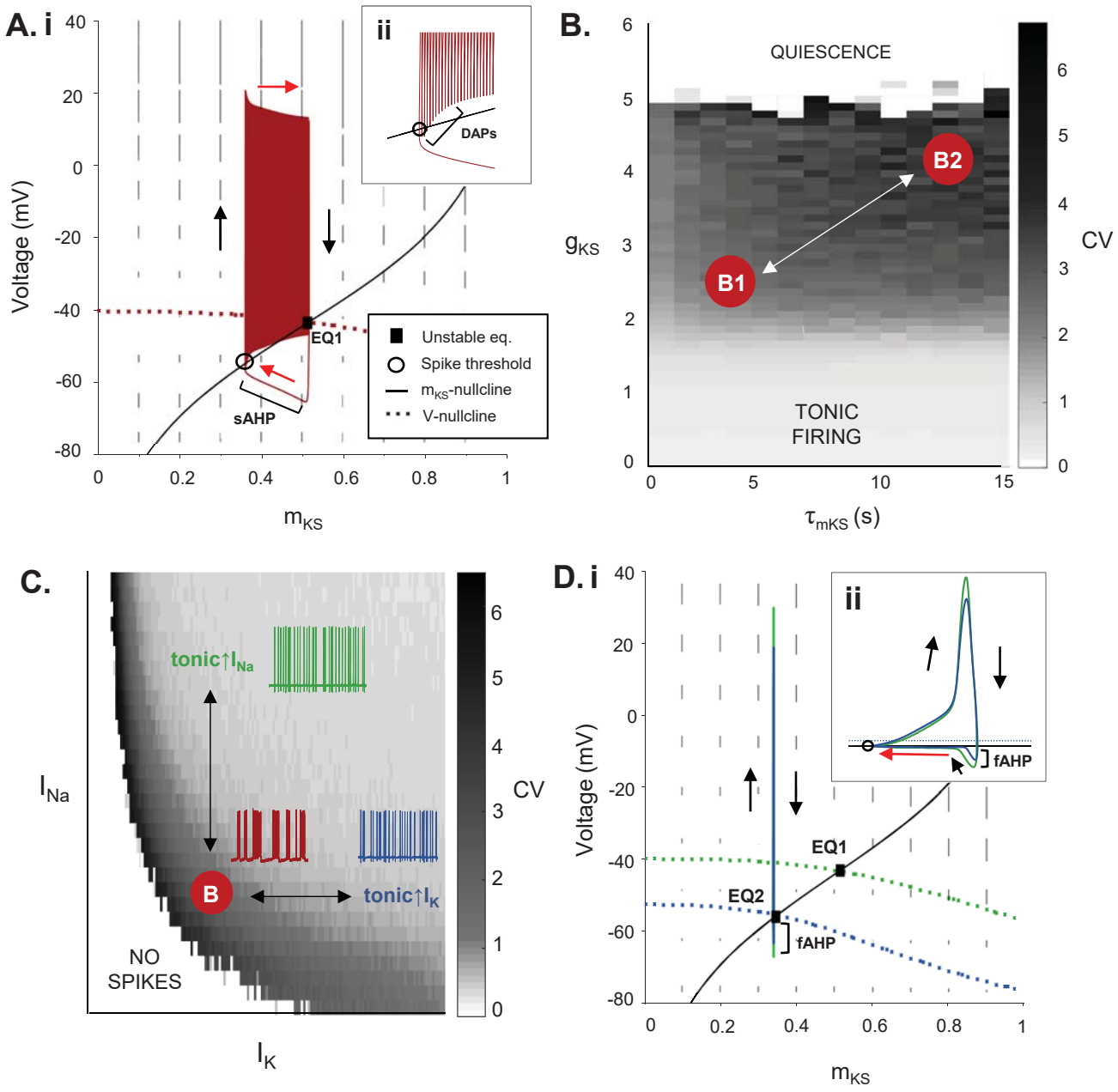

Figure 5.